

## Nanocheckerboard modulations in (NaNd)(MgW)O<sub>6</sub>

Mark W. Licurse and Peter K. Davies<sup>a)</sup>

Department of Materials Science and Engineering, University of Pennsylvania, 3231 Walnut Street, Philadelphia, Pennsylvania 19104, USA

(Received 3 June 2010; accepted 17 June 2010; published online 20 September 2010)

Data is presented for a complex structural and compositional modulation in the perovskite (NaNd)(MgW)O<sub>6</sub>. This modulation creates a large  $14a_p \times 14a_p \times 2a_p$  supercell ( $a_p \approx 3.9$  Å is the lattice parameter of the cubic perovskite aristotype) containing ordered regions with doubled (110) d-spacings in the a-b plane separated by two-dimensional periodic antiphase boundaries and accompanied by a nanocheckerboard pattern. Faint periodic modulations in Z-contrast images suggest an associated periodic variation in composition. The presence of a sodium rich impurity implies the composition of the stable perovskite is nonstoichiometric. © 2010 American Institute of Physics. [doi:10.1063/1.3490637]

Cation order/disorder transitions play a major role in adjusting the crystal structure, phase stability, and properties of many ABO<sub>3</sub> complex oxide perovskites. Compared to the numerous examples of B-site ordered perovskites, structures involving the ordering of two different cations on the A-site are relatively rare. In the few known examples the order involves a (001) layering of the A' and A'' cations.<sup>1,2</sup> The ordered A-site (A'A'')BO<sub>3</sub> perovskites have received increased attention following the observation of unusual periodic nanoscale phase separation in solid solutions of the lithium ion conducting (Nd<sub>2/3-x</sub>Li<sub>3x</sub>)TiO<sub>3</sub> system.<sup>3</sup> The tunable superlattice consists of diamondlike domains of the Li-rich end-member (NdLiTi<sub>2</sub>O<sub>6</sub>) separated by Li-free regions of Nd<sub>4/3</sub>Ti<sub>2</sub>O<sub>6</sub>. The phase separation leads to a nanocheckerboard strain pattern observed in high-resolution transmission electron microscopy (HRTEM) images. Periodic phase separated morphologies were also observed in Mn-, Cr-, and Al-substituted (Nd<sub>1/2</sub>Li<sub>1/2</sub>)TiO<sub>3</sub> solid solutions.<sup>4</sup>

Recently examples of compositional modulation were observed in Li-free perovskites. For (NaLa)(MgW)O<sub>6</sub> the modulation occurs in one dimension leading to a striped pattern of light and dark regions with a repeat distance of  $12a_p$ ; compositional analyses indicated separation into Na-rich [(NaLa)(MgW)O<sub>6</sub>] and Na-deficient [La<sub>4/3</sub>(MgW)O<sub>6</sub>] phases.<sup>5</sup> HRTEM images of (KLa)(MnW)O<sub>6</sub> provided evidence for checkerboard type modulations in another A<sup>+</sup>/A<sup>3+</sup> mixed A-site system.<sup>6</sup>

This paper focuses on the perovskite (NaNd)(MgW)O<sub>6</sub>, one of several (A'A'')(B'B'')O<sub>6</sub> perovskites with both A- and B-site ordering.<sup>7</sup> The B-site cations adopt an ordered “rocksalt-type” arrangement with an alternation of Mg<sup>2+</sup> and W<sup>6+</sup>; the A-site cations (Na<sup>+</sup>, Nd<sup>3+</sup>) adopt the usual (001) layering with  $c=2a_p$  (see Fig. 1). Samples of (NaNd)(MgW)O<sub>6</sub> were synthesized using standard ceramic methods from stoichiometric mixtures of dried Na<sub>2</sub>CO<sub>3</sub>, Nd<sub>2</sub>O<sub>3</sub>, MgO and WO<sub>3</sub> starting materials. After an initial calcine at 900 °C (3 h) all subsequent firings were conducted on pelleted samples buried in “sacrificial” powders of the same composition to minimize any loss of sodium. Equilibrium, as gauged by the absence of any changes in the powder

x-ray diffraction (PXRD) patterns, was reached after repeated grinding and heating at 1100 °C (12 h) and 1150 °C (12 h). The final samples were reheated to 1050 °C for 6 h and cooled to room temperature at 0.1 °C/min. The phase composition was characterized by a laboratory x-ray diffractometer (Rigaku GiegerFlex D/Max-B) and by synchrotron PXRD from data collected at Argonne National Laboratory with  $\lambda=0.41225$  Å. TEM analysis was conducted on a JEOL 2010F TEM/scanning transmission electron microscope (STEM) operating at 197 kV; Z-contrast images were obtained using a high-angle annular detector (54.9 mrad) in dark field STEM operating mode.

Figure 2 shows an HRTEM image and accompanying selected-area electron diffraction (SAED) pattern of (NaNd)(MgW)O<sub>6</sub> collected with the electron beam oriented along [001]. The sharp, well-defined satellites grouped around the primary perovskite reflections indicate the presence of a highly ordered superstructure with modulations along the  $g_{100}$  and  $g_{010}$  directions. The spacing of the satellites corresponds to a  $14a_p \times 14a_p$  supercell ( $\sim 5.46 \times 5.46$  nm) within the a-b plane. In the thicker regions of the grain the image is dominated by contrast from a check-

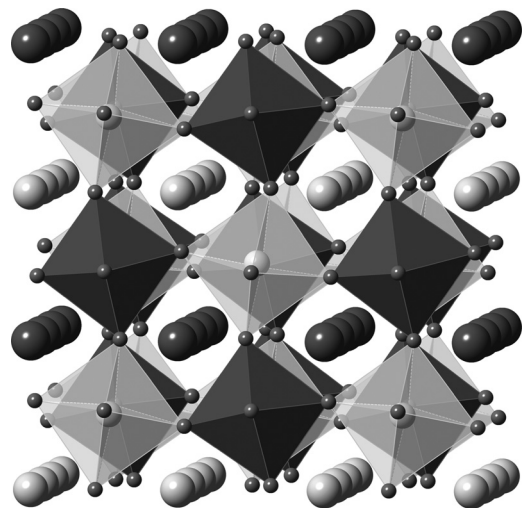


FIG. 1. Crystal structure of the double perovskite (NaNd)(MgW)O<sub>6</sub>. The light octahedra, MgO<sub>6</sub>, the darker WO<sub>6</sub>, Na<sup>+</sup> and Nd<sup>3+</sup> are represented by the light and dark spheres, respectively.

<sup>a)</sup>Electronic mail: davies@seas.upenn.edu.

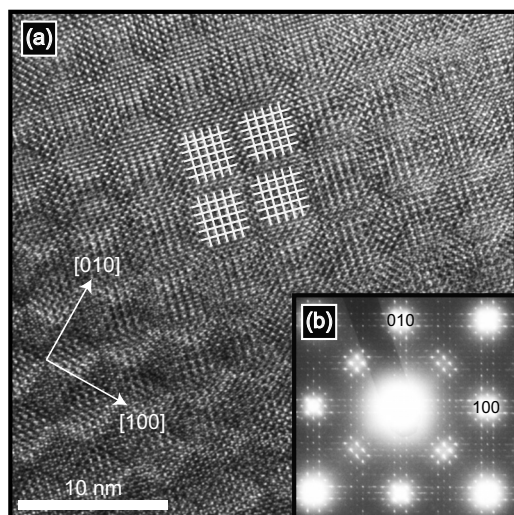


FIG. 2. (a) HRTEM image showing the checkerboard contrast along [001]. Doubling of the (110) d-spacings is highlighted by white cross-hatching; APB's are evident in the upper-right region. (b) Corresponding SAED pattern.

erboard arrangement of darker and lighter squares with edges along [100] and [010]. Although the size of the squares shows some variation, typically they correspond to  $7a_p \times 7a_p$ . The checkerboard patterns show remarkable perfection and persist across the entire grain (see Fig. 3). The morphology of the patterns for  $(\text{NaNd})(\text{MgW})\text{O}_6$  is quite different to those reported for its La counterpart, which comprise dark and light linear stripes of width  $6a_p$ .

In the thinner regions of the grain, upper right region of Fig. 2(a), the lattice image reveals a periodic arrangement of approximately square nanodomains with edges parallel to (110) and  $(1\bar{1}0)$ . Within the domains additional fringes corresponding to a doubled (110) plane d-spacing (highlighted as white cross-hatching) are evident along both (110) directions. The image also reveals an antiphase relationship between the doubled (110) spacings in adjacent domains. The antiphase boundaries (APB's) are orthogonal to each other, parallel to the {110} planes, and separated by  $7(110)a_p$ . The resultant C-centered supercell has a  $14a_p \times 14a_p$  repeat. The signature of this modulation is also evident in the diffraction

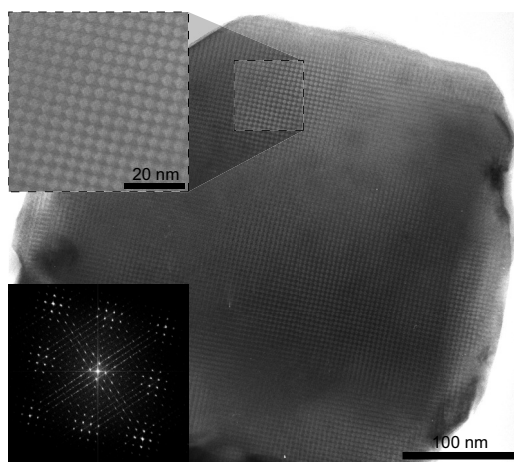


FIG. 3. Low magnification TEM image along [001] showing periodic modulation extends across entire crystal; Inset shows corresponding fast Fourier transform.



FIG. 4. [001] Z-contrast image showing a faint compositional modulation.

patterns [Fig. 2(b)], which contain four especially pronounced satellite reflections centered around the  $(h/2 \ k/2 \ 0)$  positions. The width of the APB's is difficult to fully quantify but appears to be limited to one or two perovskite unit cells. The doubled (110) fringes and periodic arrangement of APB's is very similar to the features reported for the phase-separated  $(\text{Nd}_{2/3-x}\text{Li}_{3x})\text{TiO}_3$  system. Although not mentioned in the previous study, we note the doubling of (110) and formation of APB's can also be discerned in the HRTEM images of  $(\text{NaLa})(\text{MgW})\text{O}_6$  [see Fig. 4(c), Ref. 5].

To simplify the image-contrast mechanisms, the grains were investigated using high-angle annular dark field STEM (Z-contrast imaging). The Z-contrast image in Fig. 4, collected along [001], shows a faint nanoscale compositional modulation with lighter and darker regions. The observation of this contrast implies the structural modulation in  $(\text{NaNd})(\text{MgW})\text{O}_6$  is accompanied by a periodic variation in composition.

The checkerboard modulations and domain structures in  $(\text{NaNd})(\text{MgW})\text{O}_6$  strongly resemble the phase-separated structures reported for the  $(\text{Nd}_{2/3-x}\text{Li}_{3x})\text{TiO}_3$  system. They also share several similarities to the striped patterns observed in  $(\text{NaLa})(\text{MgW})\text{O}_6$  which were argued to result from an ordered phase separation of Na-rich,  $(\text{NaLa})(\text{MgW})\text{O}_6$ , and Na-deficient,  $\text{La}_{4/3}(\text{MgW})\text{O}_6$ , end member phases.<sup>5</sup> The nanoscale structures in both of those systems also involve a periodic twinning of the  $a^-a^-c^0$  (Glazer notation) octahedral tilt system, the same tilt system reported for  $(\text{NaNd})(\text{MgW})\text{O}_6$ .<sup>8,9</sup> With these similarities it is tempting to conclude the modulations reported here for  $(\text{NaNd})(\text{MgW})\text{O}_6$  involve periodic phase separation into  $(\text{NaNd})(\text{MgW})\text{O}_6$  domains separated by Na-deficient regions of  $\text{Nd}_{4/3}(\text{MgW})\text{O}_6$ . However, if this model is correct the actual composition of the grains would have to deviate from a 1:1 Na:Nd stoichiometry.

For  $(\text{NaLa})(\text{MgW})\text{O}_6$  local fluctuations in composition and/or Na-loss during the synthesis were suggested as possible sources for the nonstoichiometric phase separated structures. However, local variations in composition are unlikely to explain the structures of the  $(\text{NaNd})(\text{MgW})\text{O}_6$  system as the formation and periodicity of the modulations patterns was not a localized phenomenon and encompassed the entire grain of every crystal imaged along [001] as seen in Fig. 3.

While sodium loss during the synthesis is possible, our preparations used sacrificial powders, a technique that is usually highly effective in suppressing component volatility. The previous preparations of  $(\text{NaLa})(\text{MgW})\text{O}_6$  and related compounds incorporated excess Na into the starting stoichiometry to compensate for potential volatilization and typically contained residual Na impurities, (e.g.,  $\text{Na}_2\text{WO}_4$ ). Even though our starting compositions were based on a stoichio-

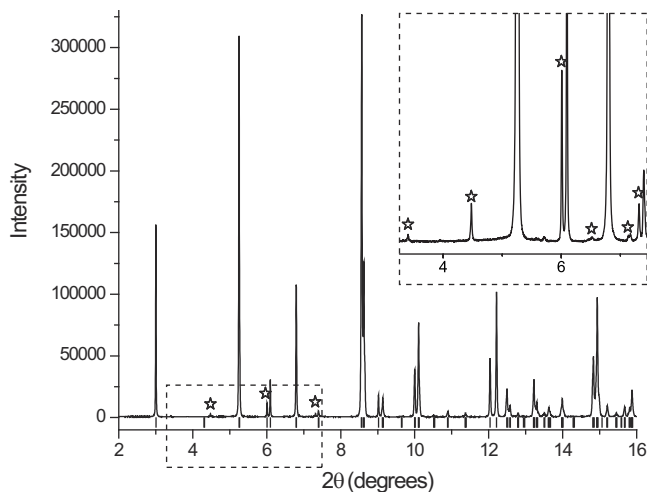


FIG. 5. Synchrotron PXRD pattern of  $(\text{NaNd})(\text{MgW})\text{O}_6$ ; stars indicate the peaks from the sodium rich impurities  $\text{Na}_2\text{WO}_4$  and  $\text{Na}_2\text{WO}_4 \cdot 2\text{H}_2\text{O}$ . Lower hash marks correspond to the expected positions based on refined lattice parameters.

metric ratio of Na:Nd:Mg:W, we also noticed the PXRD patterns of  $(\text{NaNd})(\text{MgW})\text{O}_6$  consistently contained extremely weak additional reflections at positions corresponding to  $\text{Na}_2\text{WO}_4$ . To clarify the identity of the impurity phase the samples were investigated by synchrotron PXRD. In addition to peaks for the majority perovskite phase, (indexed using a  $\sqrt{2}a_p \times \sqrt{2}a_p \times 2a_p$ ,  $P2_1/m$  cell with:  $a=5.4750$  Å,  $b=5.4868$  Å,  $c=7.8622$  Å,  $\beta=90.11^\circ$ ) the synchrotron patterns, Fig. 5, show clear evidence for small concentrations of  $\text{Na}_2\text{WO}_4$  and its hydrate,  $\text{Na}_2\text{WO}_4 \cdot 2\text{H}_2\text{O}$ . The observation of an excess Na phase confirms the effectiveness of our synthetic method in suppressing volatility; however, it also suggests the composition of the stable end-member is not  $(\text{NaNd})(\text{MgW})\text{O}_6$  but is Na (and perhaps W) deficient. The lack of stability for the stoichiometric mixed A-site end-member is strikingly similar to the  $(\text{RE})_{2/3-x}\text{Li}_{3x}\text{TiO}_3$  (RE = Nd, La) systems where “(RELi) $\text{Ti}_2\text{O}_6$ ” is also unstable and cannot be formed without trace amounts of a lithium-rich impurity.<sup>10</sup>

In summary, the structure of  $(\text{NaNd})(\text{MgW})\text{O}_6$  is comprised of ordered domains with a doubled periodicity along both (110) directions in the a-b plane. Neighboring domains have an antiphase relationship and are separated by two-dimensional periodic APB's parallel to the  $\{110\}$  planes with a  $7(110)a_p$  repeat. The resultant C-centered supercell in the a-b plane has a  $14a_p \times 14a_p$  ( $\sim 5.46 \times 5.46$  nm) periodicity. The formation of the ordered APB structure is accompanied by a checkerboard strain contrast throughout the grains. The observation of excess Na (and W) impurity phases in

samples with a bulk 1:1:1:1 Na:Nd:Mg:W ratio suggests the modulated structure is nonstoichiometric, most likely from a different local chemistry in the regions close to the APB. Understanding the origin of the doubled (110) spacing and the driving force for the formation of the periodic APB's will require additional study. The formation of periodic antiphase domains with a similar doubled (110) contrast in the  $(\text{Nd}_{2/3-x}\text{Li}_{3x})\text{TiO}_3$  system was associated with the ordering of cation displacements in the  $\text{TiO}_6$  octahedra. It is possible displacements of W could be responsible for the modulations in  $(\text{NaNd})(\text{MgW})\text{O}_6$ , though periodic twinning of the octahedral tilt system is also important in these systems.<sup>4,11</sup>

It is clear the (001) ordering of A-site cations in  $(\text{NaNd})(\text{MgW})\text{O}_6$  and other  $A^+/A^{3+}$  perovskites introduces some type of instability that produces a complex structural and compositional modulation. For the  $(\text{Nd}_{2/3-x}\text{Li}_{3x})\text{TiO}_3$  system, alterations in the bulk composition of the solid solution changed the width of the interdomain boundary regions and enabled the preparation of tunable “phase separated” checkerboard structures. The possible formation of similar tunable structures based on  $(\text{NaNd})(\text{MgW})\text{O}_6$  will require clarification of the composition of the “second-phase” APB regions.

Use of the Advanced Photon Source at Argonne National Laboratory was supported by the U. S. Department of Energy, Office of Science, Office of Basic Energy Sciences, under Contract No. DE-AC02-06CH11357. The authors thank Matthew Suchomel for assistance with the synchrotron XRD scans. This work was supported by the National Science Foundation, under Grant No. DMR0704255, and by the MRSEC Program, under Award No. DMR05-20020.

<sup>1</sup>P. K. Davies, H. Wu, A. Y. Borisevich, I. E. Molodetsky, and L. Farber, *Annu. Rev. Mater. Res.* **38**, 369 (2008).

<sup>2</sup>M. C. Knapp and P. M. Woodward, *J. Solid State Chem.* **179**, 1076 (2006).

<sup>3</sup>B. S. Gupton and P. K. Davies, *Nature Mater.* **6**, 586 (2007).

<sup>4</sup>B. S. Gupton and P. K. Davies, *J. Am. Chem. Soc.* **130**, 17168 (2008).

<sup>5</sup>S. García-Martín, E. Urones-Garrote, M. C. Knapp, G. King, and P. M. Woodward, *J. Am. Chem. Soc.* **130**, 15028 (2008).

<sup>6</sup>S. García-Martín, E. Urones-Garrote, M. C. Knapp, G. King, and P. M. Woodward, *Structural Complexity In AA'MM'O<sub>6</sub> Perovskites. A Transmission Electron Microscopy Study*, MRS Symposia Proceedings (Materials Research Society, Pittsburgh, 2008), pp. 6–11.

<sup>7</sup>G. King, S. Thimmaiah, A. Dwivedi, and P. M. Woodward, *Chem. Mater.* **19**, 6451 (2007).

<sup>8</sup>G. King, S. García-Martín, and P. M. Woodward, *Acta Crystallogr., Sect. B: Struct. Sci.* **65**, 676 (2009).

<sup>9</sup>A. M. Glazer, *Acta Crystallogr., Sect. B: Struct. Crystallogr. Cryst. Chem.* **28**, 3384 (1972).

<sup>10</sup>A. D. Robertson, S. Garcia Martin, A. Coats, and A. R. West, *J. Mater. Chem.* **5**, 1405 (1995).

<sup>11</sup>B. S. Gupton, H. Wu, and P. K. Davies, *Chem. Mater.* **20**, 2860 (2008).